Controlled-NOT gate based on the Rydberg states of surface electrons

Jun Wang, Wan-Ting He, Cong-Wei Lu, Yang-Yang Wang, Qing Ai, and Hai-Bo Wang, Beijing Normal University, Beijing 100875, China

School of Electronic Information, Xijing University, Xi'an, 710123

(Dated: March 22, 2023)

Due to the long coherence time and efficient manipulation, the surface electrons (SE) provide a perfect two-dimensional platform for quantum computation. In this work, we theoretically present a scheme to realize the controlled-NOT (CNOT) gate, by encoding the two-qubit system in the four-level Rydberg structure of SE. The state transfer is achieved by a three-level structure with an intermediate level. By simultaneously driving the SE with two external electromagnetic fields, we exploit the dark state in the electromagnetically induced transparency (EIT) effect to suppress the population of the most dissipative state and increase the robustness against dissipation. The fidelity of our scheme exceeds 0.999 with experimentally achievable parameters.

I. INTRODUCTION

Universal quantum logic gates are the key elements of quantum information processing [1, 2]. In recent years, many schemes of quantum logic gates have been proposed in various physical systems, such as superconducting qubits [3–5], nuclear magnetic resonance (NMR) systems [6, 7], cavity quantum electrodynamics (QED) [8, 9], circuit QED [10, 11], ion traps [12, 13], quantum dots [14], and nitrogen-vacancy centers in diamond [15, 16]. Among the above proposals, the controlled-NOT (CNOT) gate is one of the most attractive quantum gates, because it can be used to realize universal quantum computation with the aid of single-qubit gates [1]. A feasible quantum gate requires the operation time to be shorter than the coherent time of the system, thus the fast manipulation plays the significant role in quantum gates. Some previous works have utilized the electromagnetically induced transparency (EIT) [17] effect to reduce the influence of dissipation and accelerate the manipulation [18, 19].

The surface electron (SE) on the surface of liquid helium provides a controllable two-dimensional (2D) quantum system to study the behavior of strongly-correlated electrons. The SE is attracted by the induced image charge inside the liquid helium and concurrently repulsed by the helium atoms, and therefore the motion perpendicular to the surface is confined and forms a hydrogenlike spectrum [20]. Meanwhile, the SE can move freely parallel to the surface, forming a perfect 2D electron system free of the defects and impurities present in semiconductor devices [21]. The 2D electron system possesses the quantized orbital states when electrons are trapped in an electrostatic potential [22]. Both the Rydberg and orbital states can be coupled to the spin states of electrons [23, 24], which have a much longer coherence time than other solid materials [25], making them an excellent

resource for quantum computing. The SE can be manipulated and detected by the circuit QED architecture, which combines the superconducting coplanar-waveguide resonator and the electron trap [22, 26]. In addition, the SE can also be manipulated and transported through the microchannel devices which are fabricated on the silicon substrate and filled with the superfluid helium [27–33]. The unprecedented transport efficiency of such microchannel devices [34] manifests the applications of SE in the large-scale trapped-ion quantum computing [35].

The highly excited Rydberg state of neutral atoms is a promising candidate for quantum information processing, benefiting from its long coherence time [36] and strong long-range interactions [37]. The SE system can be used to simulate Rydberg states [20] because it has the same hydrogen-like energy spectrum as Rydberg atoms. At low temperatures, the dissipation of SE is mainly due to the height variations of the helium surface, which can be quantized as ripplons [21]. The relaxation time T_1 exceeds $10~\mu s$ at 10~m K, which is sufficiently long compared to the Rabi frequency Ω , i.e., $\Omega T_1 > 10^4~[20]$.

Here, we present a scheme to realize the CNOT gate in a single SE system. We encode the two-qubit system in the four-level Rydberg structure of SE. Since the highly excited Rydberg states are sensitive to the frequency fluctuation of the driving fields [37] and their level spacing is narrow, the direct driving for state transfer could easily cause the undesirable transitions to other neighboring states. Therefore, to accurately achieve the transition between $|10\rangle$ and $|11\rangle$, we use an intermediate level to avoid the undesired transitions to other highly excited states. By applying two driving pulses simultaneously, we exploit the dark state in the EIT effect [17, 38] to reduce the population of the most-dissipative intermediate level and increase the robustness against dissipation.

This paper is organized as follows. In Sec. II, we describe the coherent-driving scheme based on the Rydberg states of SE. In Sec. III, we compare our scheme with other schemes and show how the CNOT gate was accelerated by the two simultaneous driving fields at the same time. We also investigate the effects of detuning and dis-

^{*} hbwang@bnu.edu.cn

sipation on the fidelity. Finally, we conclude the work and give a prospect in Sec. IV. In Appendix A we provide the eigenstates and eigenvalues of the non-hermitian Hamiltonian by the perturbation theory.

II. THE MODEL

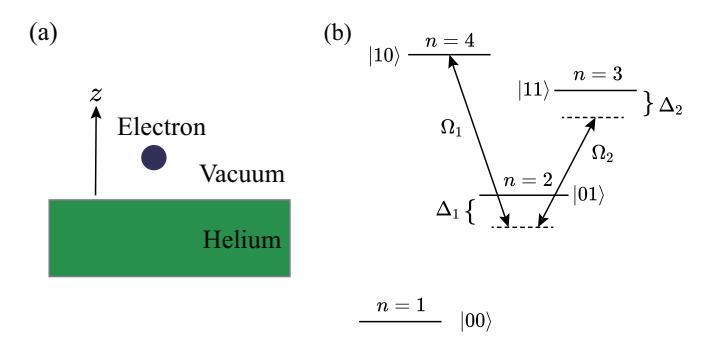


FIG. 1. Schematic diagram of the CNOT gate based on SE. (a) The SE on the surface of liquid helium. (b) The two-qubit system is encoded in the four-level SE Rydberg states, where two coherent driving fields with frequencies ω_j and Rabi frequencies Ω_j (j=1,2) are applied simultaneously. Here, Δ_1 and Δ_2 are the single-photon and two-photon detunings, respectively.

As shown in Fig. 1(a), along the direction z perpendicular to the interface, the SE is attracted by the induced image charge inside the liquid helium and concurrently repulsed by the helium atoms, and therefore the motion of the SE is confined by the hydrogen-like potential $V = -\Lambda e^2/z$ for z > 0, where e is the charge of the electron and $\Lambda = (\epsilon - 1)/[4(\epsilon + 1)]$ with the dielectric constant $\epsilon \approx 1.057$. The quantized SE states possess the hydrogen-like energy spectrum as [20, 39]

$$\varepsilon_n^{(\perp)} = -\frac{m_e e^4 \Lambda^2}{2\hbar^2 n^2} = -\frac{R}{n^2},\tag{1}$$

where m_e is the mass of the electron, the positive integer n labels the SE state, and $R \approx 0.7$ meV [20] is the Rydberg energy.

We encode the two-qubit system in the four-level Rydberg structure of the SE, as shown in Fig. 1(b). We encode the ground state with n=1 as $|00\rangle$, the first excited state with n=2 as $|01\rangle$, the second excited state with n=3 as $|11\rangle$, and the third excited state with n=4 as $|10\rangle$, respectively. The energy space ΔE_n decreases with n, so the level spacing of highly excited Rydberg states is narrow. Moreover, since the dipole moment matrix elements for the transitions between highly excited states are large, the direct transition between these states is sensitive to the frequency fluctuation of the driving fields [37]. This sensitivity of the direct manipulation of highly excited states could easily cause the undesirable transition to other neighboring states. Therefore, we use the

first excited state $|01\rangle$ as an intermediate state to realize the state swap between $|10\rangle$ and $|11\rangle$.

Two driving fields with frequencies ω_1 (ω_2) and Rabi frequencies Ω_1 (Ω_2) are used to drive the transition $|01\rangle \rightleftharpoons |10\rangle$ ($|01\rangle \rightleftharpoons |11\rangle$), as shown in Fig. 1(b). The single-photon detuning is $\Delta_1 = \omega_1 - (\omega_{10} - \omega_{01})$ and the two-photon detuning is $\Delta_2 = \omega_1 - \omega_2 - (\omega_{10} - \omega_{11})$, where ω_{01} , ω_{10} and ω_{11} are the energies of the states $|01\rangle$, $|10\rangle$ and $|11\rangle$ respectively. As the driving frequencies are largely detuned from the transitions between $|00\rangle$ and other states, we consider $|00\rangle$ to be a decoupled state. In the subspace spanned by $\{|10\rangle, |01\rangle, |11\rangle\}$, the Hamiltonian is

$$H = \omega_{10}|10\rangle\langle10| + \omega_{01}|01\rangle\langle01| + \omega_{11}|11\rangle\langle11| - \Omega_1\cos\omega_1t(|01\rangle\langle10| + |10\rangle\langle01|) - \Omega_2\cos\omega_2t(|01\rangle\langle11| + |11\rangle\langle01|),$$
 (2)

where $\hbar=1$. In the rotating frame with driving frequencies $U=\exp[i\omega_1t|01\rangle\langle01|+i(\omega_1-\omega_2)t|11\rangle\langle11|]$, under the rotating-wave approximation [40, 41], and taking $\omega_{10}=0$ as the zero point of energy, the matrix form of the Hamiltonian reads

$$H_{I} = i\frac{dU^{\dagger}}{dt}U + U^{\dagger}HU$$

$$= -\frac{1}{2} \begin{pmatrix} 0 & \Omega_{1} & 0\\ \Omega_{1} & -2\Delta_{1} & \Omega_{2}\\ 0 & \Omega_{2} & -2\Delta_{2} \end{pmatrix}.$$
(3)

The evolution of the system can be described by the quantum master equation [42]

$$\frac{\partial}{\partial t}\rho = -i[H_I, \rho] - \mathcal{L}(\rho), \tag{4}$$

where the Lindblad operator is

$$\mathcal{L}(\rho) = \kappa_1[|01\rangle\langle 01|\rho|01\rangle\langle 01| - \frac{1}{2}\{|01\rangle\langle 01|, \rho\}]$$

$$+\kappa_2[|11\rangle\langle 11|\rho|11\rangle\langle 11| - \frac{1}{2}\{|11\rangle\langle 11|, \rho\}]$$

$$+\kappa_3[|10\rangle\langle 10|\rho|10\rangle\langle 10| - \frac{1}{2}\{|10\rangle\langle 10|, \rho\}]$$
 (5)

with $\{A, B\} = AB + BA$ being the anti-commutator, and κ_1 , κ_2 and κ_3 being the dissipation rates of the energy levels $|01\rangle$, $|11\rangle$ and $|10\rangle$ respectively. Because the lifetime of the Rydberg state increases with n, i.e., $1/\kappa_n \propto n^3$ [37], we mainly consider the dissipation of the energy levels $|01\rangle$ and $|11\rangle$ and neglect the dissipation of $|10\rangle$. Recent works have provided exact and efficient quantum algorithms to simulate the quantum open system both theoretically [43] and experimentally [44], even for the non-Markovian process [45].

To solve the time evolution analytically, we neglect the quantum jump term and describe the evolution by the Schrödinger equation with the following non-Hermitian

Hamiltonian

$$H_{I}^{d} = H_{I} - i \frac{\kappa_{1}}{2} |01\rangle\langle 01| - i \frac{\kappa_{2}}{2} |11\rangle\langle 11|$$

$$= -\frac{1}{2} \begin{pmatrix} 0 & \Omega_{1} & 0\\ \Omega_{1} & -2\delta_{1} & \Omega_{2}\\ 0 & \Omega_{2} & -2\delta_{2} \end{pmatrix}, \tag{6}$$

where $\delta_1 = \Delta_1 - i\kappa_1/2$, $\delta_2 = \Delta_2 - i\kappa_2/2$. When $\delta_2 \ll \Omega_1, \Omega_2$, we take δ_2 as the perturbation term. As shown in Appendix A, the first-order approximations of the eigenvalues are

$$E_{1} \simeq \frac{\Omega_{1}^{2}}{\Omega^{2}} \delta_{2},$$

$$E_{2} \simeq \frac{\Omega}{2} + \frac{\delta_{1}}{2} + \frac{\Omega_{2}^{2}}{2\Omega^{2}} \delta_{2},$$

$$E_{3} \simeq -\frac{\Omega}{2} + \frac{\delta_{1}}{2} + \frac{\Omega_{2}^{2}}{2\Omega^{2}} \delta_{2},$$

$$(7)$$

where $\Omega = \sqrt{\Omega_1^2 + \Omega_2^2}$. The zeroth-order approximations of the eigenstates are

$$|a_{1}\rangle = \cos\theta |10\rangle - \sin\theta |11\rangle,$$

$$|a_{2}\rangle = \sin\theta \sin\phi |10\rangle + \cos\phi |01\rangle + \cos\theta \sin\phi |11\rangle, \quad (8)$$

$$|a_{3}\rangle = \sin\theta \cos\phi |10\rangle - \sin\phi |01\rangle + \cos\theta \cos\phi |11\rangle,$$

where $\tan \theta = \Omega_1/\Omega_2$ and $\tan 2\phi = \Omega/\delta_1$. It is noteworthy that $|a_1\rangle$ is a dark state since there is no population on the state $|01\rangle$ and $E_1=0$ in the zeroth-order approximation, while $|a_2\rangle$ and $|a_3\rangle$ are bright states. The time evolution of the initial state $|\psi(0)| = C_1|a_1\rangle + C_2|a_2\rangle + C_3|a_3\rangle$ is

$$|\psi(t)\rangle = C_1 e^{-iE_1 t} |a_1\rangle + C_2 e^{-iE_2 t} |a_2\rangle + C_3 e^{-iE_3 t} |a_3\rangle$$

$$= (C_1 \cos \theta e^{-iE_1 t} + C_2 \sin \theta \sin \phi e^{-iE_2 t} + C_3 \sin \theta \cos \phi e^{-iE_3 t}) |10\rangle$$

$$+ (C_2 \cos \phi e^{-iE_2 t} - C_3 \sin \phi e^{-iE_3 t}) |01\rangle$$

$$+ (-C_1 \sin \theta e^{-iE_1 t} + C_2 \cos \theta \sin \phi e^{-iE_2 t} + C_3 \cos \theta \cos \phi e^{-iE_3 t}) |11\rangle. \tag{9}$$

The key point of the CNOT gate scheme is to swap the state $|10\rangle$ for $|11\rangle$, while the population of $|01\rangle$ is small in the final state. The state swapping is based on the population oscillation. As $E_1 \ll E_2$, E_3 , the main oscillation factors are $\exp(-iE_2t)$ and $\exp(-iE_3t)$. To achieve the maximum population reversal of $|10\rangle$ and $|11\rangle$, these two oscillation terms $\exp(-iE_2t)$ and $\exp(-iE_3t)$ should have the same period. The synchronization of $\exp(-iE_2t)$ and $\exp(-iE_3t)$ requires $E_2 = -E_3$, so δ_1 and δ_2 must be much smaller than Ω , i.e.,

$$\tan \phi = 1. \tag{10}$$

Meanwhile, the oscillation term in the coefficient of $|10\rangle$ and $|11\rangle$ must be the same, which means that $\cos \theta = \sin \theta$, i.e.,

$$\Omega_1 = \Omega_2. \tag{11}$$

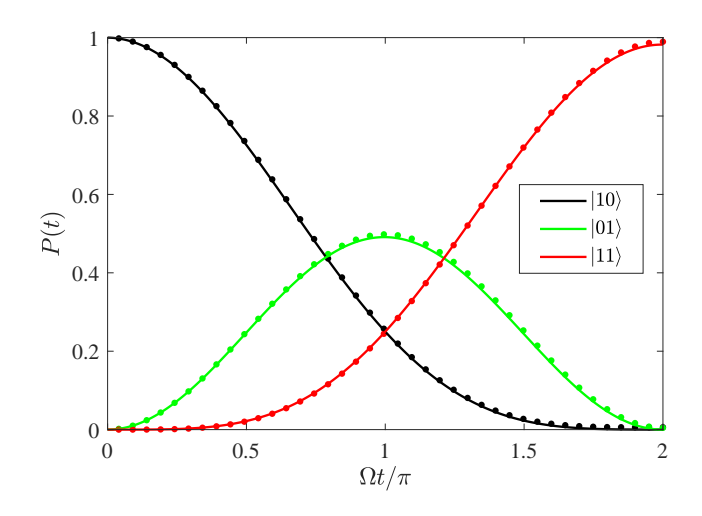


FIG. 2. The populations P(t) of different states with the initial state $|10\rangle$, with the dissipation rates $\kappa_1/\Omega=0.01$ and $\kappa_2=0.3\kappa_1$. The solid lines are the analytic solutions and the dots are the numerical solutions by the quantum master equation [46, 47].

Under these conditions, if the initial state is $|\psi(0)\rangle = |10\rangle$, the final state is

$$|\psi(t)\rangle = \left(\frac{1}{2}\cos\frac{\Omega t}{2}e^{-i\frac{2\delta_1+\delta_2}{4}t} + \frac{1}{2}e^{-i\frac{\delta_2}{2}t}\right)|10\rangle$$
$$-\frac{i}{\sqrt{2}}\sin\frac{\Omega t}{2}e^{-i\frac{2\delta_1+\delta_2}{4}t}|01\rangle$$
$$+\left(\frac{1}{2}\cos\frac{\Omega t}{2}e^{-i\frac{2\delta_1+\delta_2}{4}t} - \frac{1}{2}e^{-i\frac{\delta_2}{2}t}\right)|11\rangle. \tag{12}$$

If the initial state $|\psi(0)\rangle = |01\rangle$, the final state is

$$|\psi(t)\rangle = -\frac{i}{\sqrt{2}}\sin\frac{\Omega t}{2}e^{-i\frac{2\delta_1+\delta_2}{4}t}|10\rangle$$

$$+\cos\frac{\Omega t}{2}e^{-i\frac{2\delta_1+\delta_2}{4}t}|01\rangle$$

$$-\frac{i}{\sqrt{2}}\sin\frac{\Omega t}{2}e^{-i\frac{2\delta_1+\delta_2}{4}t}|11\rangle. \tag{13}$$

If the initial state $|\psi(0)\rangle = |11\rangle$, the final state is

$$|\psi(t)\rangle = \left(\frac{1}{2}\cos\frac{\Omega t}{2}e^{-i\frac{2\delta_1+\delta_2}{4}t} - \frac{1}{2}e^{-i\frac{\delta_2}{2}t}\right)|10\rangle$$
$$-\frac{i}{\sqrt{2}}\sin\frac{\Omega t}{2}e^{-i\frac{2\delta_1+\delta_2}{4}t}|01\rangle$$
$$+\left(\frac{1}{2}\cos\frac{\Omega t}{2}e^{-i\frac{2\delta_1+\delta_2}{4}t} + \frac{1}{2}e^{-i\frac{\delta_2}{2}t}\right)|11\rangle. \tag{14}$$

The time evolution of different initial states is shown in Fig. 2. Since the 0 K radiative lifetime $\tau^{(0)}$ of the alkalis Rydberg state is proportional to the cube of the principal quantum number n: $\tau^{(0)} \propto n^3$ [37], we take $\kappa_1/\Omega=0.01$ and $\kappa_2/\kappa_1=2^3/3^3\approx 0.3$ for simplicity. The maximum population reversal between $|10\rangle$ and $|11\rangle$ is reached when $\Omega t=2\pi$. The analytical solutions are in good agreement with the numerical solutions.

III. FIDELITY ANALYSIS

Since the driving frequencies are far detuned from the transition between $|00\rangle$ and other states, we consider $|00\rangle$ to be a decoupled state. From the time evolution in Eq. (12)-(14), the maximum population reversal between $|10\rangle$ and $|11\rangle$ is achieved when $\Omega t = 2\pi$. The state fidelity F between the final state $\rho(t)$ and the ideal target state ρ_i is defined as [48, 49]

$$F = \left(\text{Tr}\sqrt{\sqrt{\rho_i}\rho(t)\sqrt{\rho_i}}\right)^2. \tag{15}$$

In our coherent-driving scheme, two driving fields interact with the SE simultaneously, with the dark and bright states being used equally for the state transfer. The maximum fidelity is achieved when $t=2\pi/\Omega$, as shown in Fig. 3(c). For comparison, we show the result of the two-step driving scheme in Fig. 3(b). We derive the population reversal between $|10\rangle$ and $|01\rangle$ by the first driving pulse $\Omega_1(t)$, and then derive the population reversal between $|01\rangle$ and $|11\rangle$ by the second driving pulse $\Omega_2(t)$. The maximum fidelity is achieved when $t=2\sqrt{2}\pi/\Omega$, which is longer than the coherent-driving scheme. In addition, the two-step driving scheme can only achieve the one-way state transfer based on the driving pulse sequence, but a NOT-gate requires the bidirectional transfer with the same driving pulse sequence.

In Sec. II, we have found that Δ_1 need to be much smaller than Ω in order to synchronize the oscillation terms $\exp(-iE_2t)$ and $\exp(-iE_3t)$. When the single-photon resonance condition is invalid, the fidelity of the state transfer decreases, as shown in Fig. 4. It is noteworthy that the oscillation period changes with Δ_1 . Thus, the fidelity is calculated at the maximum in the first period. On the other hand, when Δ_2 becomes large, the perturbation method is invalid, but the evolution of the states can still be derived from the master equation. As shown in Fig. 4, when the two-photon resonance condition is invalid, the fidelity of the state transfer decreases because the EIT effect is suppressed.

Figure 3(c) only shows the fidelity of the state transfer with the input state $|10\rangle$. In Fig. 5 we present the state fidelity with different input states. The fidelity matrix corresponds to the characteristic of the CNOT gate. When the control bit is $|0\rangle$, the target bit remains in the initial state. When the control bit is $|1\rangle$, the target bit flips.

To demonstrate the characteristic of the entire gate, we calculate the gate fidelity which is defined as [50, 51]

$$F = \frac{1}{N} |\text{Tr}(e^{i\phi} U_r^{\dagger}) U_i|, \tag{16}$$

where N is the dimension of the Hilbert space, U_i is the ideal gate operation, U_r is the real operation in our scheme, and ϕ is a global phase to maximize F. Since the transitions between $|00\rangle$ and other states are negligible, we can analytically derive the operation matrix of the

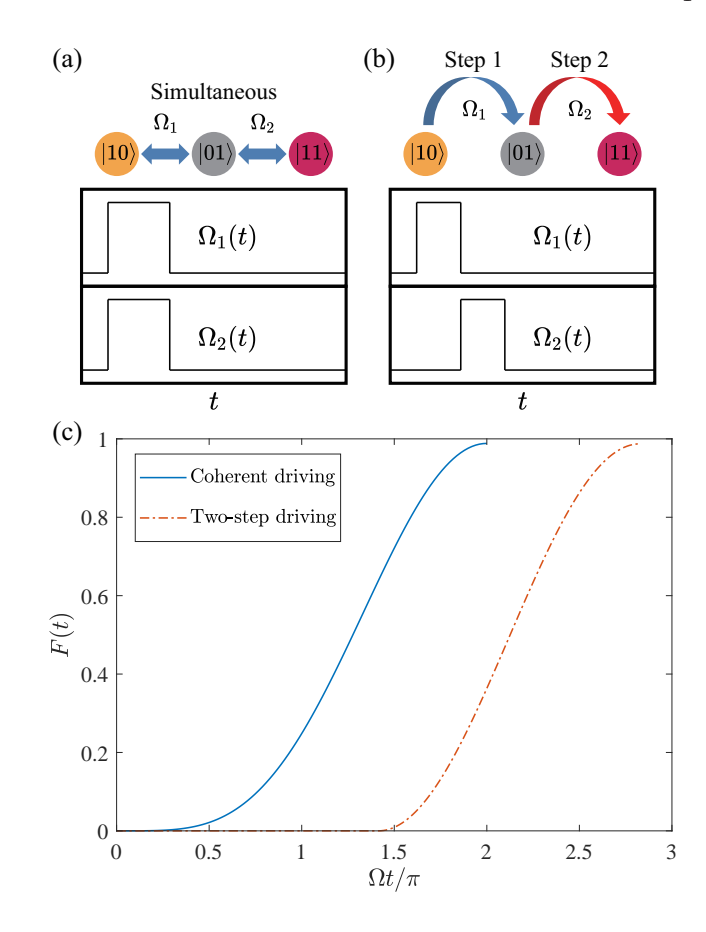


FIG. 3. (a) Schematic diagram of the coherent-driving scheme. (b) Schematic diagram of the two-step driving scheme. (c) The fidelity F of the state transfer in schemes (a)-(b), while the dissipation rates are the same as in Fig. 2.

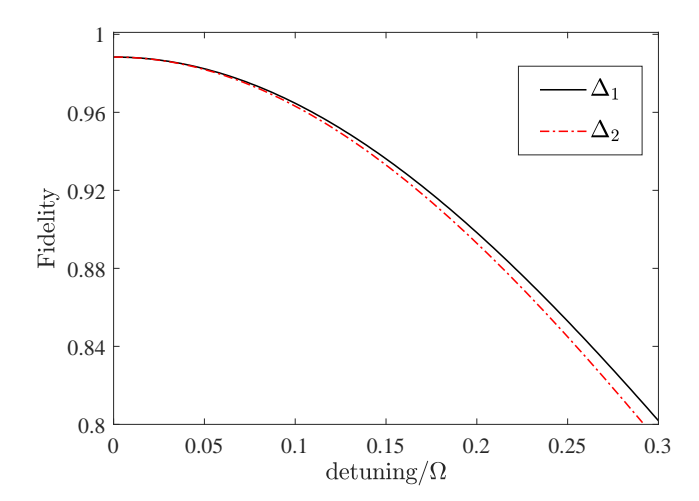


FIG. 4. State fidelity versus the single-photon (two-photon) detuning Δ_1 (Δ_2). The dissipation rates are the same as in Fig. 2. The solid (solid-dot) line shows the dependence on Δ_1 (Δ_2) with $\Delta_2 = 0$ ($\Delta_1 = 0$).

CNOT gate in our scheme from the evolution of different

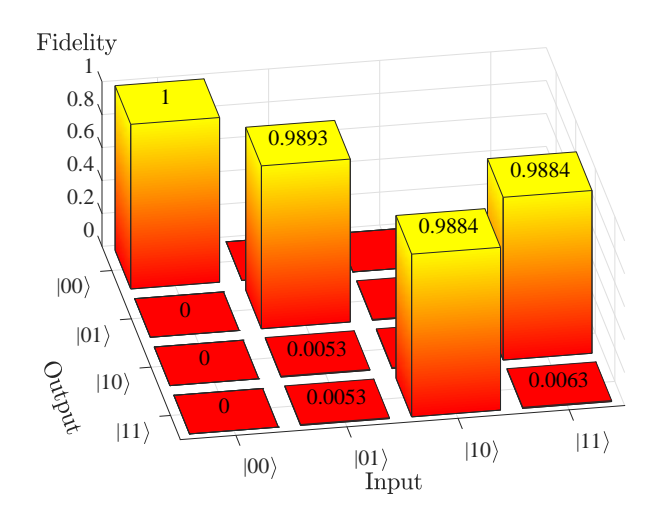


FIG. 5. The state fidelity F with different input states. For each input state, the bar shows the fidelity between the output state in our scheme and the ideal output state. The dissipation rates are the same as in Fig. 2.

initial states:

$$U_r = \begin{pmatrix} 1 & 0 & 0 & 0 \\ 0 & a & 0 & 0 \\ 0 & 0 & b & c \\ 0 & 0 & c & b \end{pmatrix}, \tag{17}$$

where

$$a = e^{-\frac{(2\kappa_1 + \kappa_2)\pi}{4\Omega}},$$

$$b = \frac{1}{2}e^{-\frac{(2\kappa_1 + \kappa_2)\pi}{4\Omega}} - \frac{1}{2}e^{-\frac{\kappa_2\pi}{2\Omega}},$$

$$c = \frac{1}{2}e^{-\frac{(2\kappa_1 + \kappa_2)\pi}{4\Omega}} + \frac{1}{2}e^{-\frac{\kappa_2\pi}{2\Omega}}.$$
(18)

This formula is obtained by an additional phase operation on $|01\rangle$, $|10\rangle$ and $|11\rangle$, which adds a π phase to these three energy levels. Compared to the ideal CNOT gate

$$U_i = \begin{pmatrix} 1 & 0 & 0 & 0 \\ 0 & 1 & 0 & 0 \\ 0 & 0 & 0 & 1 \\ 0 & 0 & 1 & 0 \end{pmatrix}, \tag{19}$$

the fidelity of U_r is

$$F = \frac{1}{4}|\text{Tr}(U_r^T U_i)| = \frac{1+a}{4} + \frac{c}{2}.$$
 (20)

In Fig. 6 we analyze the effect of dissipation on the gate fidelity. The dissipation rate κ_1 varies proportionally with κ_2 . When $\kappa_2/\Omega < 10^{-3}$ the fidelity is larger than 0.995, and F = 0.9997 with parameters $\Omega/\kappa_2 = 10^4$ which is experimentally achievable [20].

IV. CONCLUSION AND REMARKS

In this work, we present a scheme to realize the CNOT gate in the four-level Rydberg structure of SE. We use a

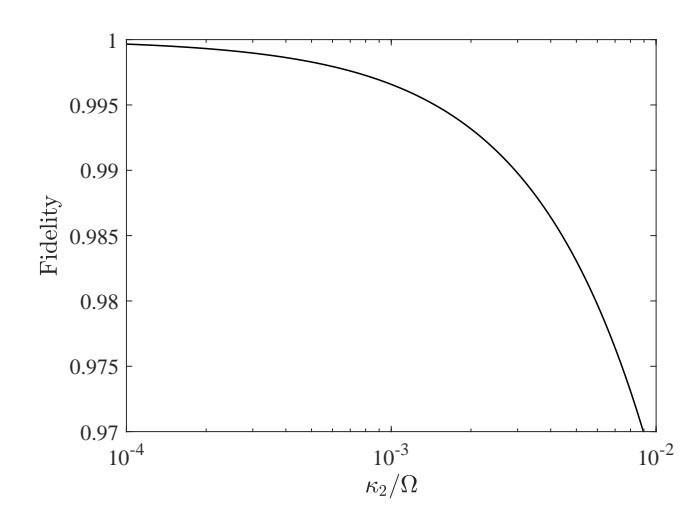


FIG. 6. The gate fidelity between the gate in our scheme and the ideal CNOT gate under different dissipation rates with $\kappa_2 = 0.3\kappa_1$.

three-level structure to realize the state transfer. By applying two driving pulses simultaneously, we exploit the dark state in the EIT effect to suppress the population of the most-dissipative state and increase the robustness against dissipation [52]. We obtain the time evolution of the system both analytically and numerically. We optimize the Rabi frequencies and the detunings of the driving fields to achieve the maximum population exchange of $|10\rangle$ and $|11\rangle$. The optimal state transfer requires that both the single-photon and the two-photon resonances are satisfied. We also calculate the fidelity of the state transfer and of the entire gate. The fidelity can exceed 0.999 with experimentally-achievable parameters [20].

In our scheme, the transition between $|10\rangle$ and $|11\rangle$ involves a three-level structure whose configuration can be the ladder type, V type, or Λ -type [17]. The choice of configuration depends on the dissipation rates of the different levels. Because the configuration of our scheme is based on the properties of Rydberg states whose lifetime increases with the energy level [37], we choose the V-type configuration to consider the most dissipative state as the intermediate state and use the EIT effect to suppress the population on this state.

The strong long-range interaction between highly excited Rydberg states [37] is another possible candidate for the realization of two-qubit quantum gates [19]. Our scheme demonstrates the advantages of precise manipulation of highly excited Rydberg states with narrow energy space, and therefore provides potential applications in the schemes based on the long-range interaction of highly excited Rydberg states. Meanwhile, since the Rydberg states of SE can be coupled to the spin states [23, 24], our scheme provides heuristic insight for the quantum information processing tasks that combine the Rydberg states and the spin states to achieve longer coherence time.

ACKNOWLEDGMENTS

This work is supported by the National Natural Science Foundation of China under Grant No. 61675028 and the Interdiscipline Research Funds of Beijing Normal University. Q. Ai is supported by the Beijing Natural Science Foundation under Grant No. 1202017 and the National Natural Science Foundation of China under Grant Nos. 11674033, 11505007, and Beijing Normal University under Grant No. 2022129. Y. Y. Wang is supported by the Natural Science Basic Research Program of Shaanxi under Grant No. 2023-JC-QN-0092.

Appendix A: Eigenvalues from the perturbation method

Assuming that $E_n = -x/2$, the secular equation of Eq. (6) is

$$x[x^{2} + 2(\delta_{1} + \delta_{2})x + 4\delta_{1}\delta_{2} - \Omega^{2}] - 2\Omega_{1}^{2}\delta_{2} = 0, \quad (A1)$$

where $\Omega = \sqrt{\Omega_1^2 + \Omega_2^2}$. To solve the secular equation, we assume δ_2 as a perturbation term and

$$x_j \approx x_{0j} + A_j \delta_2.$$
 (A2)

The zero-order terms satisfies

$$x_{0j}[x_{0j}^2 + 2(\delta_1 + \delta_2)x_{0j} + 4\delta_1\delta_2 - \Omega^2] = 0,$$
 (A3)

- [1] A. Barenco, C. H. Bennett, R. Cleve, D. P. DiVincenzo, N. Margolus, P. Shor, T. Sleator, J. A. Smolin, and H. Weinfurter, "Elementary gates for quantum computation," Phys. Rev. A 52, 3457 (1995).
- [2] T. Sleator and H. Weinfurter, "Realizable universal quantum logic gates," Phys. Rev. Lett. 74, 4087 (1995).
- [3] Y. Makhlin, G. Schön, and A. Shnirman, "Quantumstate engineering with josephson-junction devices," Rev. Mod. Phys. 73, 357 (2001).
- [4] T. Yamamoto, Y. A. Pashkin, O. Astafiev, Y. Nakamura, and J. S. Tsai, "Demonstration of conditional gate operation using superconducting charge qubits," Nature 425, 941 (2003).
- [5] Y. X. Liu, J. Q. You, L. F. Wei, C. P. Sun, and F. Nori, "Optical selection rules and phase-dependent adiabatic state control in a superconducting quantum circuit," Phys. Rev. Lett. 95, 087001 (2005).
- [6] J. A. Jones, M. Mosca, and R. H Hansen, "Implementation of a quantum search algorithm on a quantum computer," Nature 393, 344 (1998).
- [7] G. R. Feng, G. F. Xu, and G. L. Long, "Experimental

and the solutions are

$$x_{01} = 0,$$

$$x_{02} = -\delta_1 - \delta_2 - \sqrt{(\delta_1 - \delta_2)^2 + \Omega^2}$$

$$\simeq -\delta_1 - \delta_2 - \Omega - \frac{\delta_1 - \delta_2}{2\Omega} (\delta_1 - \delta_2)$$

$$\simeq -\delta_1 - \delta_2 - \Omega,$$

$$x_{03} = -\delta_1 - \delta_2 + \sqrt{(\delta_1 - \delta_2)^2 + \Omega^2}$$

$$\simeq -\delta_1 - \delta_2 + \Omega + \frac{\delta_1 - \delta_2}{2\Omega} (\delta_1 - \delta_2)$$

$$\simeq -\delta_1 - \delta_2 + \Omega.$$
(A4)

The approximation is valid when $\delta_1, \delta_2 \ll \Omega$. Thus, the secular equation is transformed into

$$(x - x_{01})(x - x_{02})(x - x_{03}) - 2\Omega_1^2 \delta_2 = 0.$$
 (A5)

Inserting $x_j \approx x_{0j} + A_j \delta_2$, we can obtain

$$A_{1} = \frac{2\Omega_{1}^{2}}{(x_{01} - x_{02})(x_{01} - x_{03})} \simeq -\frac{2\Omega_{1}^{2}}{\Omega^{2}},$$

$$A_{2} = \frac{2\Omega_{1}^{2}}{(x_{02} - x_{01})(x_{02} - x_{03})} \simeq \frac{\Omega_{1}^{2}}{\Omega^{2}},$$

$$A_{3} = \frac{2\Omega_{1}^{2}}{(x_{03} - x_{01})(x_{03} - x_{02})} \simeq \frac{\Omega_{1}^{2}}{\Omega^{2}},$$
(A6)

and the eigenvalues to the first-order approximation as

$$E_1 \simeq \frac{\Omega_1^2}{\Omega^2} \delta_2,$$

$$E_2 \simeq \frac{\Omega}{2} + \frac{\delta_1}{2} + \frac{\Omega_2^2}{2\Omega^2} \delta_2,$$

$$E_3 \simeq -\frac{\Omega}{2} + \frac{\delta_1}{2} + \frac{\Omega_2^2}{2\Omega^2} \delta_2.$$
(A7)

- realization of nonadiabatic holonomic quantum computation," Phys. Rev. Lett. **110**, 190501 (2013).
- [8] Q. A. Turchette, C. J. Hood, W. Lange, H. Mabuchi, and H. J. Kimble, "Measurement of conditional phase shifts for quantum logic," Phys. Rev. Lett. 75, 4710 (1995).
- [9] A. Rauschenbeutel, G. Nogues, S. Osnaghi, P. Bertet, M. Brune, J. M. Raimond, and S. Haroche, "Coherent operation of a tunable quantum phase gate in cavity qed," Phys. Rev. Lett. 83, 5166 (1999).
- [10] I. Chiorescu, P. Bertet, K. Semba, Y. Nakamura, C. J. P. M. Harmans, and J. E. Mooij, "Coherent dynamics of a flux qubit coupled to a harmonic oscillator," Nature 431, 159 (2004).
- [11] L. DiCarlo, J. M. Chow, J. M. Gambetta, L. S. Bishop, B. R. Johnson, D. I. Schuster, J. Majer, A. Blais, L. Frunzio, S. M. Girvin, and Schoelkopf R. J., "Demonstration of two-qubit algorithms with a superconducting quantum processor," Nature 460, 240 (2009).
- [12] J. I. Cirac and P. Zoller, "Quantum computations with cold trapped ions," Phys. Rev. Lett. 74, 4091 (1995).
- [13] J. F. Poyatos, J. I. Cirac, and P. Zoller,

- "Quantum gates with "hot" trapped ions," Phys. Rev. Lett. 81, 1322 (1998).
- [14] X. Q. Li, Y. W. Wu, D. Steel, D. Gammon, T. H. Stievater, D. S. Katzer, D. Park, C. Piermarocchi, and L. J. Sham, "An all-optical quantum gate in a semiconductor quantum dot," Science 301, 809 (2003).
- [15] F. Jelezko, T. Gaebel, I. Popa, M. Domhan, A. Gruber, and J. Wrachtrup, "Observation of coherent oscillation of a single nuclear spin and realization of a two-qubit conditional quantum gate," Phys. Rev. Lett. 93, 130501 (2004).
- [16] H. R. Wei and F. G. Deng, "Compact quantum gates on electron-spin qubits assisted by diamond nitrogen-vacancy centers inside cavities," Phys. Rev. A 88, 042323 (2013).
- [17] M. Fleischhauer, A. Imamoglu, and J. P. Marangos, "Electromagnetically induced transparency: Optics in coherent media," Rev. Mod. Phys. 77, 633 (2005).
- [18] Y. D. Wang and A. A. Clerk, "Using interference for high fidelity quantum state transfer in optomechanics," Phys. Rev. Lett. 108, 153603 (2012).
- [19] K. McDonnell, L. F. Keary, and J. D. Pritchard, "Demonstration of a quantum gate using electromagnetically induced transparency," Phys. Rev. Lett. 129, 200501 (2022).
- [20] P. M. Platzman and M. I. Dykman, "Quantum computing with electrons floating on liquid helium," Science 284, 1967 (1999).
- [21] E. Kawakami, A. Elarabi, and D. Konstantinov, "Relaxation of the excited Rydberg states of surface electrons on liquid helium," Phys. Rev. Lett. 126, 106802 (2021).
- [22] G. Koolstra, G. Yang, and D. I. Schuster, "Coupling a single electron on superfluid helium to a superconducting resonator," Nat. Commun. 10, 5323 (2019).
- [23] E. Kawakami, A. Elarabi, and D. Konstantinov, "Image-charge detection of the Rydberg states of surface electrons on liquid helium," Phys. Rev. Lett. **123**, 086801 (2019).
- [24] D. I. Schuster, A. Fragner, M. I. Dykman, S. A. Lyon, and R. J. Schoelkopf, "Proposal for manipulating and detecting spin and orbital states of trapped electrons on helium using cavity quantum electrodynamics," Phys. Rev. Lett. 105, 040503 (2010).
- [25] S. A. Lyon, "Spin-based quantum computing using electrons on liquid helium," Phys. Rev. A 74, 052338 (2006).
- [26] X. J. Zhou, G. Koolstra, X. F. Zhang, G. Yang, X. Han, B. Dizdar, X. H. Li, R. Divan, W. Guo, K. W. Murch, Schuster D. I., and Jin D. F., "Single electrons on solid neon as a solid-state qubit platform," Nature 605, 46 (2022).
- [27] P. Glasson, V. Dotsenko, P. Fozooni, M. J. Lea, W. Bailey, G. Papageorgiou, S. E. Andresen, and A. Kristensen, "Observation of dynamical ordering in a confined Wigner crystal," Phys. Rev. Lett. 87, 176802 (2001).
- [28] H. Ikegami, H. Akimoto, and K. Kono, "Nonlinear transport of the Wigner solid on superfluid ⁴He in a channel geometry," Phys. Rev. Lett. 102, 046807 (2009).
- [29] D. G. Rees, I. Kuroda, C. A. Marrache-Kikuchi, M. Höfer, P. Leiderer, and K. Kono, "Point-contact transport properties of strongly correlated electrons on liquid helium," Phys. Rev. Lett. 106, 026803 (2011).
- [30] H. Ikegami, H. Akimoto, D. G. Rees, and K. Kono, "Evidence for reentrant melting in a quasi-one-dimensional

- Wigner crystal," Phys. Rev. Lett. 109, 236802 (2012).
- [31] D. G. Rees, N. R. Beysengulov, J. J. Lin, and K. Kono, "Stick-slip motion of the Wigner solid on liquid helium," Phys. Rev. Lett. 116, 206801 (2016).
- [32] D. G. Rees, N. R. Beysengulov, Y. Teranishi, C. S. Tsao, S. S. Yeh, S. P. Chiu, Y. H. Lin, D. A. Tayurskii, J. J. Lin, and K. Kono, "Structural order and melting of a quasi-one-dimensional electron system," Phys. Rev. B 94, 045139 (2016).
- [33] A. O. Badrutdinov, D. G. Rees, J. Y. Lin, A. V. Smorodin, and D. Konstantinov, "Unidirectional charge transport via ripplonic polarons in a three-terminal microchannel device," Phys. Rev. Lett. 124, 126803 (2020).
- [34] F. R. Bradbury, M. Takita, T. M. Gurrieri, K. J. Wilkel, Kevin Eng, M. S. Carroll, and S. A. Lyon, "Efficient clocked electron transfer on superfluid helium," Phys. Rev. Lett. 107, 266803 (2011).
- [35] D. Kielpinski, C. Monroe, and D. J. Wineland, "Architecture for a large-scale ion-trap quantum computer," Nature 417, 709 (2002).
- [36] T. F. Gallagher, Rydberg Atoms (Cambridge University Press, 1994).
- [37] M. Saffman, T. G. Walker, and K. Mølmer, "Quantum information with Rydberg atoms," Rev. Mod. Phys. 82, 2313 (2010).
- [38] Y. Y. Wang, J. Qiu, Y. Q. Chu, M. Zhang, J. M. Cai, Q. Ai, and F. G. Deng, "Dark state polarizing a nuclear spin in the vicinity of a nitrogen-vacancy center," Phys. Rev. A 97, 042313 (2018).
- [39] Y. Monarkha and K. Kono, Two-Dimensional Coulomb Liquids and Solids (Springer Science & Business Media, 2004).
- [40] M. O. Scully and M. S. Zubairy, Quantum Optics (Cambridge University Press, 1997).
- [41] Q. Ai, Y. Li, H. Zheng, and C. P. Sun, "Quantum anti-zeno effect without rotating wave approximation," Phys. Rev. A 81, 042116 (2010).
- [42] H. P. Breuer and F. Petruccione, The Theory of Open Quantum Systems (Oxford University Press, 2002).
- [43] N. N. Zhang, M. J. Tao, W. T. He, X. Y. Chen, X. Y. Kong, F. G. Deng, N. Lambert, and Q. Ai, "Efficient quantum simulation of open quantum dynamics at various Hamiltonians and spectral densities," Front. Phys. 16, 51501 (2021).
- [44] B. X. Wang, M. J. Tao, Q. Ai, T. Xin, N. Lambert, D. Ruan, Y. C. Cheng, F. Nori, F. G. Deng, and G. L. Long, "Efficient quantum simulation of photosynthetic light harvesting," npj Quantum Inf. 4, 52 (2018).
- [45] X. Y. Chen, N. N. Zhang, W. T. He, X. Y. Kong, M. J. Tao, F. G. Deng, Q. Ai, and G. L. Long, "Global correlation and local information flow in controllable non-Markovian open quantum dynamics," npj Quantum Inf. 8, 22 (2022).
- [46] J. R. Johansson, P. D. Nation, and F. Nori, "Qutip: An open-source python framework for the dynamics of open quantum systems," Comput. Phys. Commun. 183, 1760–1772 (2012).
- [47]J. Johansson, Р. R., D. Nation, F. Nori, "Qutip 2: Α python framework for of quantum systems," dynamics open the Comput. Phys. Commun. 184, 1234–1240 (2013).
- [48] A. Uhlmann, "The "transition probability" in the state space of a *-algebra," Rep. Math. Phys. 9, 273 (1976).

- [49] R. Jozsa, "Fidelity for mixed quantum states," J. Mod. Opt. 41, 2315 (1994).
- [50] J. P. Palao and R. Kosloff, "Quantum computing by an optimal control algorithm for unitary transformations," Phys. Rev. Lett. 89, 188301 (2002).
- [51] C. Z. Wu, B. Qi, C. L. Chen, and D. Y. Dong, "Robust
- learning control design for quantum unitary transformations," IEEE Trans. Cybern. $\bf 47,\ 4405$ (2017).
- [52] H. B. Huang, J. J Lin, Y. X Yao, K. Y Xia, Z. Q. Yin, and Q. Ai, "Optical nonreciprocity in rotating diamond with nitrogen-vacancy color centers," Ann. Phys. (Berlin) 534, 2200157 (2022).